Journal of Drug Delivery Science and Technology 99 (2024) 105956

Contents lists available at ScienceDirect

Journal of Drug Delivery Science and Technology

journal homepage: www.elsevier.com/locate/jddst

Stabilization of cationic liposomes using hyaluronic acid-modified gold nanoparticles by post-microfluidics conjugation approach for drug delivery applications

Sarvenaz Pakian [a], Ahmad Mirkani [a], Hamid Sadeghi-Abandansari [b], Mohammad-reza Nabid [a,*]

[a] Department of Polymer and Materials Chemistry, Faculty of Chemistry & Petroleum Sciences, Shahid Beheshti University, Tehran, Iran
[b] Department of Cell Engineering, Cell Science Research Center, Royan Institute for Stem Cell Biology and Technology, ACECR, Tehran, Iran

ARTICLE INFO

Keywords:
Cationic liposomes
Microfluidics
5-Fluorouracil (5-FU)
Hydrodynamic flow focusing
Gold nanoparticles (AuNPs)
Hyaluronic acid

ABSTRACT

lipid-based nanoparticles (LNPs), particularly liposomes, have gained prominence throughout the pharmaceutical sector as a hopeful means for transporting a range of therapeutic agents. Improving LNPs stability is crucial in pharmaceuticals, and drug delivery systems to ensure their effectiveness and reliability. The current research was undertaken to design a pH-responsive hyaluronic acid-modified gold nanoparticle-stabilized cationic liposome (SPC/DOPE/DOTAP) system (HA-SH/AuNPs@liposomes) to improve the stability of liposomes. This was achieved through a post-microfluidics conjugation technique to encapsulate the 5-fluorouracil (5-FU) anticancer drug, usually employed in nonmelanoma skin cancer (NMSC) treatment. Microfluidics is an emerging technology that can be employed as a powerful tool for designing nanoscale liposomes with highly uniform size distributions and acceptable colloidal stability. Utilizing a microfluidics toroidal mixer, affixed HA-SH/AuNPs (size: 12.56 ± 1.65 nm) to positively charged liposomes (size: 75 ± 0.68 nm and PDI: 0.032 ± 0.0021). These liposomes exhibited strong stability, limited fusion propensity, and minimal cargo release at neutral pH. The gold stabilizers detached in an acidic environment, releasing encapsulated therapeutic agents. The dynamic light scattering (DLS) analysis results indicate that HA-SH/AuNPs@Liposomes (size: 102.2 ± 1.3 nm and PDI: 0.11 ± 0.01) exhibit greater stability than bare liposomes over 4 weeks at 4 °C. This enhanced stability can be attributed to the presence of HA-SH/AuNPs in the liposomal structure. This research outlines a systematic method to optimize the size rapidly and PDI of liposomes by employing the Design of Experiments (DoE). The results highlighted that utilizing both the microfluidic technique and gold nanoparticle-stabilized liposomes offers benefits for creating controlled drug release formulations. This approach leads to enhanced biopharmaceutical characteristics and improved scalability of liposomal formulations.

1. Introduction

Nanomedicine has witnessed remarkable progress in clinical applications since the late 20th century, owing to its unique merits in terms of biocompatibility, potency, and novel therapeutic possibilities [1]. Nanoparticulate technologies, especially lipid-based nanoparticles (LNPs), have transformed drug delivery by enabling targeted release, enhanced stability, and reduced adverse effects [2]. These nanoparticles are constructed using lipids, which are natural components of cell membranes and exhibit excellent biocompatibility [3]. LNPs can be tailored to encapsulate a wide range of therapeutic agents, including small molecules, nucleic acids, and proteins, offering versatility in drug delivery [4]. The lipid bilayer structure of these nanoparticles can protect the encapsulated payload from physiological degradation, enable interaction with cell membranes, and also allow surface modifications for stability, tissue targeting, and extended circulation in the bloodstream [5]. Liposomes, an earlier form of LNPs, serve as a highly adaptable nanocarrier platform. These structures can take on the forms of multi-layered or single-layered vesicles, efficiently trapping lipophilic drugs in the lipid layer and hydrophilic drugs in the internal aqueous compartment [6]. While liposomes present numerous advantages as delivery vehicles, two key limitations hinder their reproducible formation for biomedical applications with potential clinical translation. The primary and major obstacle could be attributed to the difficulties

* Corresponding author.
E-mail addresses: s_pakian@sbu.ac.ir (S. Pakian), ahmad.mirkani@yahoo.com (A. Mirkani), sadeghi.chem89@gmail.com (H. Sadeghi-Abandansari), m-nabid@sbu.ac.ir (M.-r. Nabid).

https://doi.org/10.1016/j.jddst.2024.105956
Received 21 January 2024; Received in revised form 28 May 2024; Accepted 7 July 2024
Available online 8 July 2024

associated with mass production and scaling up, and the second obstacle is related to the stability of liposomes during manufacturing and storage [7]. In traditional batch processes, the lipid thin-film hydration method is commonly utilized for the production of liposomes [8]. By employing this method, the formation of large and polydisperse particles occurs. Therefore, it becomes imperative to undergo a subsequent size reduction process, such as extrusion, sonication, or homogenization, to regulate the size of liposomes for pharmaceutical applications. Optimal size can enhance the ability of liposomes to penetrate specific tissues or target cells, improving the overall efficacy of drug delivery. Conversely, excessively large liposomes may face challenges in cellular internalization. The stability of liposomal formulations is also influenced by size [9,10]. These size-tuning processes can occasionally lead to the breakage of encapsulated molecules due to physical stress [11]. The use of microfluidic systems in liposome production might overcome these major challenges. Microfluidics is a powerful technology that enables precise control over fluid flow, mixing, and droplet formation, leading to enhanced batch-to-batch reproducibility and scalability [12,13]. In the context of liposome production, microfluidic platforms allow for the continuous and controlled mixing of lipids and encapsulated payloads, resulting in more uniform and consistent liposomal formulations. The microscale dimensions of these systems facilitate rapid and efficient mixing, reducing the formation of non-uniform liposomes or aggregates [14]. Moreover, microfluidic techniques can be combined with on-chip monitoring and characterization methods, enabling real-time quality control and optimization of liposome production parameters [15]. The initial utilization of microfluidic mixing to produce liposomes was documented by Jan et al. [16]. In their work, the researchers employed hydrodynamic focusing on lipids dissolved in alcohol miscible with water, placed between two aqueous buffer streams in a microfluidic cartridge. This method yielded uniform liposomes with their size regulated by the flow rate. Recently, a novel mixing architecture called NxGen has been introduced, which consists of a series of bifurcating mixers for scalable, non-turbulent mixing [17]. These toroidal mixers, also known as bifurcating mixers, create chaotic movement in the fluid as it travels. The channels divide into two, follow distinct path lengths, and eventually recombine. This process leads to quick mixing in a single-layer device, driven by substantial centrifugal forces [18]. As a second issue, the use of liposomes is typically constrained by their natural instability, caused by uncontrollable fusion among liposomes. This instability results in a short shelf life, unwanted loss of payload, and unexpected mixing [19]. The nanoparticle-stabilized liposomes, also known as hybrid liposomes, have emerged as a promising approach to overcome the stability limitations of conventional liposomes [20,21]. By incorporating nanoparticles within the liposomal structure, these hybrid systems can enhance the physical and chemical stability of liposomes. This method has successfully increased liposome stability, however the relatively hard membrane that results from nanoparticle attachment severely inhibits drug release from these liposomes. Gold nanoparticles (AuNPs) are generating significant attention in the field of nanotherapeutics due to their non-toxic nature, water-friendly characteristics, customizable size and charge, and modifiable surface chemistry [22]. Zhang et al. have regulated the fusion behavior of liposomes by attaching carboxyl-modified gold nanoparticles to the external surface of phospholipid liposomes [23]. The attached AuNPs are successful in preventing the fusion of liposomes at a neutral pH. However, in acidic conditions (e.g., pH < 5), the stabilizing effect of the gold particles diminishes, leading to their detachment from the liposomes and a subsequent resumption of liposome fusion activity. In addition, due to reactive oxygen species (ROS) activity, AuNPs have shown some toxicity for some types of cells such as retinal pigment epithelial cells [24]. B. B. Karakocak and et al. were coated AuNPs with hyaluronic acid (HA) and showed that HA coating significantly enhanced the biocompatibility of AuNPs by mitigating ROS pathways known to lead to cell death. They also confirmed that receptors on cell surfaces, for HA, enabled HA-Au NPs entry in the cells via CD44 receptors, acting as a Trojan horse for the larger particles [25]. D. Pornpattananangkul and et al. modified gold nanoparticles with chitosan (AuChi) and the attached AuChi to the surface of liposomes. This novel liposome formulation not only effectively prevented the fusing of liposomes, but also prevented the undesirable payload release in regular storage or physiological environments [19]. HA possesses hydrophilic functional groups that can form a protective layer around the nanoparticles, creating steric repulsion between particles. This repulsion prevents close contact and aggregation, thereby enhancing the nanoparticles' stability in solution. In this study, we hypothesized that binding of hyaluronic acid-modified gold nanoparticles (HA-SH/AuNPs) to the surface of liposomes would prevent liposomes from fusing, undesirable payload release, and also improve cellular uptake through HA receptor-mediated endocytosis. The main objective of this study is to present an enhanced cationic liposomal formulation tailored for the topical delivery of 5-FU to achieve localized effects in dermal fibroblast tissue within the skin layers. Accordingly, we created a liposome formulation composed of SPC/DOPE/DOTAP, and surface modification was done by HA-SH/AuNPs. This formulation was designed for the targeted topical release of elevated amounts of the chemotherapy drug 5-fluorouracil (5-FU), used as a representative drug model. To equip cationic liposomes with HA-SH/AuNPs, a post-microfluidics conjugation approach by electrostatic adsorption mechanism was conducted [26,27]. This type of surface modification technique prevents the inherent infusion of liposomes. The negatively charged HA-SH/AuNPs bind to the positively charged surfaces of liposomes through electrostatic attraction. By examining various attributes of HA-SH/AuNPs@Liposomes, including particle size, zeta potential, encapsulation efficiency (EE), drug loading capacity (DL), and stability, we aim to establish a foundation for potential utilization as a localized drug delivery system in skin cancer treatment. HA-SH/AuNPs@Liposomes as a topical drug delivery system, particularly in the form of liposomal ointments, show significant potential for treating various skin diseases (nonmelanoma skin cancer (NMSC)). Their ability to enhance drug penetration, provide sustained release, and offer targeted therapy makes them a valuable option for optimizing therapeutic outcomes in dermatological applications. The outcomes of this project hold promise for shaping future advancements in this direction.

2. Materials and methods

2.1. Materials

L-α-phosphatidylcholine (SPC, 95 %), 1,2-dioleoyl-*sn*-glycero-3-phospho ethanol amine (DOPE), and 1,2-dioleoyl-3-trimethylammonium-propane (DOTAP) were purchased from Lipoid Co (Germany). Hyaluronic acid (HA, sodium salt, Cosmetic grade, Mw = 10000 Da) was obtained from Bloomage Freda Biopharm Corporation (Shandong, China). Tetrachloroauric (III) acid ($HAuCl_4.3H_2O \geq$ 99 % trace metal basis), trisodium citrate dihydrate (SC, ≥99 %), N-hydroxysuccinimide (NHS, 99 %), potassium carbonate (≥99 %), tannic acid (TA, MW 1701, ACS reagent), 1-ethyl-3-(3- dimethyl aminopropyl) carbodiimide hydrochloride (EDCI, 99 %), 5, 5′-dithiobis-(2-nitrobenzoic acid) (DTNB, 99 %), Triton™ X-100, 5-Fluorouracil (5-FU, ≥99 %, HPLC, powder, Mw = 130.08, at room temperature, the solubility of 5-FU is 12.2 mg/ml in water), 3-(4, 5-dimethylthiazol-2-yl)-2, 5-diphenyl tetrazolium bromide (MTT), and cysteamine hydrochloride (CSA·HCl, 99 %) were purchased from Sigma-Aldrich Co (USA). Other chemicals were used at analytical grade and ultrapure water (18.2 MΩ) was used for all procedures.

2.2. Chemical characterization and instrumentation

The morphology of the nanoparticles was measured by a Philips EM 208S transmission electron microscope (TEM) operated at an accelerating voltage of 100 kV. The microstructure was assessed using field

emission scanning electron microscopy (FE-SEM) equipment (Tescan Vegan). UV–visible spectra were acquired with a Shimadzu UV-2400 spectrophotometer. Particle size and polydispersity index (PDI) of the samples were determined by dynamic light scattering (DLS) using a Zetasizer Nano ZS (Malvern) with a backscattering detection angle of 173, a He/Ne laser that emits at 633 nm, and a 4.0 mW power source and HORIBA DLS-7100, Japan. Apparent zeta potential and surface charge were determined using the Zeta SizerVer.7.11 (Malvern Instruments Ltd., Malvern, UK). Samples were placed in a clear disposable zeta cell after suitable dilution in filtered distilled water at 25 °C. FT-IR analyses were determined via a Nicolet spectrophotometer model Nexus 470 ESP™. Proton nuclear magnetic resonance (^{1}H NMR) spectra were recorded on a BRUKER DRX-300 AVANCE spectrometer. The X-ray diffraction (XRD) analyses were performed with a STOE XD-3A X-ray diffractometer, operating with a parallel Cu-Kα radiation at $\lambda = 1.54056$ Å, in the range of 2θ from 10° to 80°. The cooling centrifuge Sigma 3-18 KS instrument was applied in the present study (3-18 KS; Sigma, Aachen, Germany).

2.3. Gold nanoparticles synthesis (AuNPs)

AuNPs were prepared by using the Inverse Turkevich method with some modifications [28]. In a 250 mL three-necked round-bottom flask, a 150 mL freshly prepared reducing solution of SC (2.2 mM) with 0.1 mL of TA (2.5 mM) and 1 mL of K_2CO_3 (150 mM) was heated with a heating mantle and vigorously stirred. At a temperature of 70 °C, 1 mL of $HAuCl_4.3H_2O$ with a concentration of 25 mM was injected into the solution. In less than 10 s, the color of the solution changed from its initial state to black-gray, and then within the next 1–2 min, it changed into an orange-red. To ensure the full reaction of the gold precursor, the solution was maintained at 70 °C for an additional 5 min. The resulting particles were narrowly spread, negatively charged, and stable for weeks (~10 nm, 3×10^{12} NPs/mL). The pH of the reducing solution reached to 10 after the addition of 1 mM of K_2CO_3, and fell to a pH of 8 after the addition of $HAuCl_4.3H_2O$ in the reaction mixture.

2.4. Synthesis of Thiolated Hyaluronic Acid (HA-SH)

The HA-SH was synthesized using the following procedure as a representative example [29]. Initially, 400 mg of HA and 230 mg (2 mmol) of NHS were dissolved completely in 80 mL of deionized water while stirring at room temperature. The mixture was then treated with 383 mg (2 mmol) of EDCI, added in solid form, and allowed to react for 2 h to activate the carboxylic group of HA. After that, 114 mg (1 mmol) of CSA·HCl was dissolved in 10 mL of deionized water and added to the mixture. During the reaction process, the pH of the solution was maintained at 4.75 by using 1.0 M NaOH or 1.0 M HCl as necessary. The mixed solution was stirred for 24 h before being transferred to the dialysis tubing (cut off: 3500 Da) and dialyzed vigorously for 48 h against diluted HCl solution (pH 3.5) containing 100 mM NaCl. The HA-SH solid was eventually produced by lyophilizing the acidified solution. The chemical structures of HA-SH and HA were determined by ^{1}H NMR and FT-IR spectra.

2.5. Synthesis of HA-SH/AuNPs complex

The HA-SH was attached to the surface of gold through a chemical process in which the thiol group of the HA-SH interacted with the gold atoms at a molecular level [30,31]. Briefly, HA-SH solution (5 mg/mL) was prepared by mixing HA-SH powder in Milli-Q water and stirring until complete dissolution. Afterward, 4 μL of the solution containing HA-SH was introduced to 1 mL of the purified AuNPs. The resulting mixture was vigorously mixed using a vortex to ensure thorough blending and uniformity. Following a 20-min incubation period, the AuNPs solution was buffered by gradually adding a concentrated PBS solution (6 × PBS, pH 7.0, 2 M NaCl) over 2 h. The final salt concentration was adjusted to 0.3 M. The above solution was then incubated for another 24 h to form a stable sulfur–metal bond. The resultant HA-SH/AuNPs were centrifuged and washed three times with 0.1 M PBS solution (pH 7.0) to remove unbound HA-SH molecules. UV-VIS spectra were acquired after 1 and 24 h to check particle stability and assess changes in the surface plasmon resonance (SPR). The solution was stored at room temperature.

2.6. Preparation and optimization of 5-FU loaded cationic liposomes (SPC/DOPE/DOTAP)

2.6.1. Thin-film hydration process

Cationic liposomes were prepared according to the thin-film hydration process reported by Bangham et al. [32]. In short, stock solutions for each lipid (SPC, DOTAP, DOPE) were prepared in chloroform and stored at −20 °C. The lipid solutions were combined in the specified proportions (SPC/DOPE/DOTAP 50:25:25 M ratio), mixed, and then dried to form a thin film. This process was carried out using a rotary evaporator under a vacuum of 650 mm Hg for 2 h. The dehydrated lipid film was rehydrated with PBS buffer for 40 min, reaching a concentration of 20 mM at 30 °C, exceeding its phase transition temperature. Subsequently, the mixture underwent bath sonication for 5 min to create small unilamellar empty liposomes. 5-FU loaded liposomes were also prepared using a thin-film hydration method. For passive loading, the dried lipid films were hydrated using an aqueous 5-FU solution of 1 mg/mL for 2 h at 40 °C on a rotary evaporator. The resulting liposomal formulation underwent bath sonication for 20 min at 25 °C, and then it was extruded through 200 nm membrane filters (Nuclepore™, GE Healthcare, Chicago, IL, USA) using a LiposoFast® Extruder device (Avestin Inc., Ottawa, ON, Canada). This extrusion process, consisting of 15 cycles, was conducted at 65 °C to produce small unilamellar vesicles (SUVs).

2.6.2. Microfluidic process

Liposomes were produced using desktop Nanosynthesizer® equipment (INSIGHT®, NanoSynthes® Co.) that allowed rapid mixing of formulation solutions in a microfluidic-based cartridge. The microfluidic cartridge had two inlets that merged into a micro-channel. One inlet facilitated the introduction of lipid mixtures dissolved in ethanol (EtOH), while the other inlet allowed for the addition of buffer solutions (D-PBS). The variable exhibited by the benchtop Nano assembler allowed the control of total flow rate (TFR: 7–20 mL/min) and flow rate ratio (FRR: 1:1 to 1:5 EtOH: D-PBS). Initial lipid concentrations used were 5–25 mM depending on the formulation and lipid ratio is variable (55:20:25, 55:25:20, 50:25:25. SPC, DOTAP, DOPE). Lipids were dissolved in ethanol and mixed with an aqueous phase. For the production of 5-FU loaded liposomes, initial concentrations (1 mg/mL in PBS; 10 mM, pH 7.4) of 5-FU were reused as the aqueous phase. The liposome formulations were collected from the chamber outlet and dialyzed at room temperature against PBS buffer for removal of residual solvent. To achieve the lowest PDI and particle size, the identification of the optimum conditions for synthesizing such a liposome formulation is essential. To optimize the process variables affecting the PDI and particle size of liposomes and reduce the total number of experiments (cost of research), the experiment design method was employed.

2.7. DoE approach

2.7.1. Screening of formulation by taguchi design

The screening of formulation was performed by evaluating the effect of different factors on particle size and PDI. Liposomal formulations were screened using the Taguchi design. Several factors can influence the reduction of PDI, including the lipid ratio, the total lipid content, TFR, and FRR. To design the experiment, relevant values were selected for each factor based on the results of preliminary studies and previous research. To ensure appropriate allocation of values, three different levels were assigned to each factor, with levels 1 to 3 specified in

Table 1
Various levels of each factor and their values (Process parameters for screening.).

Factor	Symbol	Level 1	Level 2	Level 3
Lipid ratio	LR	50:25:25	55:25:20	55:20:25
Total Lipid Content	TLC	5	10	20
Total Flow Rate	TFR	7	12	20
Flow Rate Ratio	FRR	1:1	1:3	1:5

Table 1.

2.7.2. Assign factors using an orthogonal array

To create a perfect liposome sample using the microfluidic method, a standard orthogonal array was created using the Taguchi experimental design method. To achieve this, a set of nine experiments was conducted using an L_9 orthogonal array, as shown in Table 2. The resulting PDI and particle size values for each experiment were determined to identify the optimal outcome. The data obtained from the experiments were then subjected to statistical analysis using the widely used software, Minitab. The adoption of this methodology ensures the reliability and accuracy of the experiment's outcomes.

2.7.3. Optimization of reaction parameters

In this research, the Taguchi method was used as an experimental design to investigate how different parameters affect the quality of the process. The goal was to pinpoint the most crucial factors influencing the quality of the end product while minimizing the number of experiments required in the microfluidic method. This approach aimed to enhance performance, cut down on costs, and save time. This methodology utilizes orthogonal arrays based on factorial design to effectively lay out the experiments, including the selection of factors and their corresponding levels. Specifically, the reaction variables investigated in this study included the LR, TLC, TFR, and FRR, which are commonly observed factors in the synthesis of liposomes at microfluidic method. To investigate the effects of these variables, three levels were chosen for each factor, as detailed in Table 1. An orthogonal array is denoted by the symbol L_9. Based on the objective function of the study, the most effective factor and its most important level were determined and presented in Table 1. The range analysis of the orthogonal experiment results revealed that the optimal value of LR was at level 1 (50:25:25). Furthermore, the TLC at level 3 (20 mM), indicated the optimum value.

Table 2
Screening of formulation by Taguchi design.

	Independent variables				Dependent variables	
Test number	Lipid ratio	Total Lipid	TFR	FRR	Particle size (nm)	PDI
1	Level 1	Level 1	Level 1	Level 1	85.0 ± 0.98	0.070 ± 0.0022
2	Level 1	Level 2	Level 2	Level 2	86.0 ± 0.52	0.069 ± 0.0045
3	Level 1	Level 3	Level 3	Level 3	78.0 ± 0.81	0.033 ± 0.0036
4	Level 2	Level 1	Level 2	Level 3	82.0 ± 0.64	0.065 ± 0.0041
5	Level 2	Level 2	Level 3	Level 1	80.0 ± 0.62	0.052 ± 0.0049
6	Level 2	Level 3	Level 1	Level 2	76.0 ± 0.97	0.063 ± 0.0034
7	Level 3	Level 1	Level 3	Level 2	81.0 ± 0.69	0.062 ± 0.0033
8	Level 3	Level 2	Level 1	Level 3	80.0 ± 0.78	0.059 ± 0.0041
9	Level 3	Level 3	Level 2	Level 1	80.9 ± 0.85	0.055 ± 0.0026
10[a]	Level 1	Level 3	Level 3	Level 3	75 ± 0.68	0.032 ± 0.0021

[a] Indicates optimized formulation.

The optimal value of the TFR was found at level 3 (20 mL/min), and for the FRR, the optimal value was at level 3 (1:5). Based on the results, it can be inferred that the most effective factors that influence the experiment's outcome are ranked in the following order: TLC > TFR > FRR > LR.

To further improve the quality of the liposomes produced based on the component levels determined through the Taguchi design and microfluidic method, an extra sample was created (referred to as sample 10). This sample was formulated using the optimal level of each factor that was identified in this study. The purpose of this was to attain a low PDI. The optimal levels of the factors were identified to be TLC level 3, TFR level 3, FRR level 3, and LR level 1, and the resultant liposome was named sample 10.

2.8. Preparation of HA-SH/AuNPs@Liposomes

To prepare HA-SH/AuNPs@Liposomes, the pH levels of both AuNPs and liposome suspensions were adjusted to 7.4 using NaOH. Subsequently, the liposomes and HA-SH/AuNPs at the desired molar ratio were combined and vortexed for 10 min. The hydrodynamic size and surface zeta potential of the prepared liposomes and HA-SH/AuNPs@Liposomes were assessed by DLS analysis. The morphology and structure of the HA-SH/AuNPs@Liposomes were characterized by TEM equipped with a cold cathode field emission electron source and a turbo-pumped main chamber. Samples for TEM characterization were prepared by spreading a solution containing the HA-SH/AuNPs@Liposomes onto the surface of a copper grid coated with a carbon film.

2.9. 5-FU entrapment efficiency and drug loading by centrifugal ultrafiltration method

The EE% and DL% of the cationic liposomes that were produced with thin-film and microfluidic process, was determined by the centrifugal ultrafiltration method [33,34]. Briefly, the 5-FU loaded liposomes were centrifuged for 1 h at 10000 rpm using centrifugal filter tubes (molecular weight (MW) cutoff = 10 kDa; Millipore) at 4 °C. The nanoparticles were separated from the aqueous phase, and the free 5-FU was analyzed in the supernatant. The UV–Vis spectrophotometry method was used to measure the free drug concentration in the samples after centrifugation and supernatant collection. For direct measurement of drugs within the liposomes, 5-FU inside the liposomes was determined using 0.5 % Triton-X as the lysing agent. Absorbance at 266 nm was measured by a UV–vis spectrometer and the EE% and DL% were determined from a calibration curve. The EE % and DL% were calculated using the following equations [35,36].

$$\%EE = \frac{\text{Weight of the drug in nanoparticles}}{\text{Weight of the feeding drugs}} \times 100 \quad (1)$$

$$\%DL = \frac{\text{Weight of the drug in nanoparticles}}{\text{Weight of the nanoparticles}} \times 100 \quad (2)$$

2.10. In vitro drug release study

The in vitro release of drug-loaded liposomal formulations was determined using homemade vertical Franz-type glass diffusion cells (available diffusion area = 1.8 cm^2). A cellulose membrane (molecular weight cutoff of 12 KDa) was mounted between the donor and receptor compartments. The membrane was soaked in double-distilled water for 12 h before mounting in the Franz diffusion cell. Respective liposomal formulations (5-FU/Liposome, 5-FU/HA-SH/AuNPs@Liposomes) were placed in the donor compartment and dialyzed against a receptor medium consisting of PBS (pH 7.4, 5.5 and 4). The stirring rate and temperature were kept at 300 rpm and 37 °C, respectively. The samples were removed in 10 days. Each experiment was repeated in triplicate. In

all instances, the incubation medium was replaced with a fresh one daily. Samples for 5-FU analysis were taken from receptors and analyzed via the UV-VIS spectrophotometer method at wavelengths of 266 nm.

2.11. Physicochemical and structural characterization of liposomes

2.11.1. Particle size, PDI, and zeta potential

The particle sizes and PDI of liposomes at the concentration of 0.2 mM were measured by DLS. The Zeta potential values also were evaluated by electrophoretic light scattering.

2.11.2. Morphology

The external structure and surface morphology of the liposomes were observed by the FE-SEM technique and the internal structure of the particles was displayed using the TEM technique. For FE-SEM analysis, a drop of the liposomal suspension was placed on a clean mica surface and dried at 30 °C. Then, it was sputter-coated with platinum in a Quorum MIRA3 Sputter Coater (Quorum Technologies) and examined with a FEI Quanta FE-SEM. For TEM analysis, a drop of the samples (~5 μL) was placed on a copper grid coated with a carbon film. The negative staining was performed with a 2 % solution of uranyl acetate for ~10 s and then blotted dry.

2.11.3. Stability studies

The physical stability of liposomes refers to their ability to maintain their structural integrity and size distribution over time. It's important to monitor changes in zeta potential and size as indicators of liposome stability. The stability of optimized liposomal formulations (HA-SH/AuNPs@Liposomes and bare liposomes) was evaluated over 4 weeks. In summary, the formulations were stored at both 4 °C and 37 °C, and samples were collected at specific time intervals. These samples were then analyzed for size (Z-average), zeta potential, and PDI.

2.12. In vitro biocompatibility evaluation

The biocompatibility of different systems, including free liposomes (The concentration range tested was between 1 and 30 (mM)), HA-SH, AuNPs, HA-SH/AuNPs, and HA-SH/AuNPs@Liposomes, was assessed using an MTT assay. The MTT assay measures cell viability and compares it with a blank control, where cells are cultured without any system in the culture medium. The Human Keratinocyte Cells (HaCaT) (HaCaT cell line was purchased from Pasteur Institute, Tehran, Iran). were cultured in DMEM containing 10 % fetal bovine serum (FBS, Gibco), and 1 % penicillin/streptomycin (Thermo Fisher) supplements and incubated in 37 °C humidified incubator containing 5 % CO_2. All of the systems were sterilized by a 0.2 mm syringe filter and HA-SH/AuNPs@Liposomes were formed by simple mixing of liposome solutions with HA-SH/AuNPs solutions in a sterile environment. Free liposomes in different concentrations, HA-SH, AuNPs, HA-SH/AuNPs (in the concentration that was used in the final system), and HA-SH/AuNPs@Liposomes were placed in a well, and cells (5×10^5 cells/100 μL solution) were cultured on the solutions for 3 days. The cytotoxicity was assessed using an MTT reagent according to the manufacturer's instructions. The absorbance of samples was measured at 570 nm and viability (%) was calculated as follows:

$$\text{Viability}\ (\%) = ([\text{A}]\text{test} / [\text{A}]\text{control}) \times 100 \quad (3)$$

Where [A]test is the absorbance of the sample cells and [A]control is the absorbance of the untreated cells. The data are presented as mean ± standard deviation (SD) of three experiments.

2.13. In vitro cytotoxicity evaluation

The epidermal carcinoma (A431) cell line was purchased from Pasteur Institute, Tehran, Iran. A431 cells were grown using DMEM high glucose medium, supplemented with 10 % fetal bovine serum and incubated at 37 °C in an atmosphere of 5 % CO_2. In vitro, cell viability in the presence of 5-FU (1 mg. mL^{-1}), free HA-SH/AuNPs@Liposomes, and drug-loaded HA-SH/AuNPs@Liposomes (5-FU, 1 mg. mL^{-1}) was determined using MTT assay. For this, the cells were trypsinized, plated in a 96-well microplate (1×10^4 cells/well) and incubated for 24 h at 37 °C in a 5 % CO_2 atmosphere. Then, the cells were rinsed with saline, protected from light, added with the MTT solution (250 μg/mL) and incubated for 4 h at 37 °C in 5 % CO_2. We subsequently discarded the solutions in the wells and added 200 μL of DMSO to solubilize formazan crystals. Quantification was performed by measuring the absorbance values in a microplate reader at 570 nm (as mentioned in equation (3)).

3. Results and discussion

3.1. Synthesis of HA-SH functionalized AuNPs complexes (HA-SH/AuNPs)

In this study, HA-SH (MW 10 kDa) was used to surface-passivate AuNPs synthesized using an Inverse Turkevich method, as shown in Scheme 1 [37]. As a first step, HA-SH was prepared using a carbodiimide-mediated chemical method (Scheme 1A) [38]. Initially, the carboxylic group of HA was reacted with NHS to prepare an HA-NHS active ester, using EDCI as a condensing agent. Subsequently, HA-NHS was further reacted with CSA•HCl to synthesize the hyaluronic acid thiol-modified polymer (HA-SH). Following this, to obtain a pure product, the raw HA-SH product underwent extensive dialysis against a dilute aqueous solution of HCl (pH 3.5). This process prevented the thiol groups from reacting with each other and forming disulfide bonds. Finally, the solution was lyophilized to obtain solid HA-SH. In this reaction, the amidation reaction between HA-COOH and CSA-NH_2 was significantly influenced by the molar ratio of HA, EDCI, and CSA•HCl (molar ratio: HA/EDCI/CSA•HCl = 1/4/4) during the feeding process. The degree of thiol was 60.56 %, which was measured by a modified Ellman method [39]. Following this procedure, DTNB reacted with the free thiol group, producing a product with a distinct absorption peak at 412 nm in the UV test. This characteristic peak could be utilized for the quantitative determination of the free thiol group. The presence of conjugated thiol groups was confirmed using the ^{1}H NMR spectrum, and the typical spectra of both native HA and HA-SH were illustrated in Scheme 1B. In comparison to the spectrum of native HA, it is clear that new resonant peaks of HA-SH have appeared at 2.65 ppm and 2.75 ppm. These peaks correspond to the methylene protons of the –$CH_2$$CH_2$SH and -$CH_2$$CH_2$SH, respectively, in the spectrum of the HA-SH polymer. In the second step, citrate-stabilized AuNPs were synthesized to react with HA-SH. The schematic in Scheme 1C illustrates the molecular interaction and surface chemistry of AuNPs stabilized with HA-SH.

In this study, we leverage recent advancements in the kinetic control of seeded-growth synthesis for citrate-stabilized metal nanoparticles. This approach enables the production of AuNPs with precise control over morphology and nanometric size resolution ranging from 3.5 to 10 nm. Controlled nucleation of (~10 nm, 3×10^{12} NPs/mL) AuNPs is achieved by the combined use of two competing reducing agents: TA and SC. The utilization of these two reducing agents for the synthesis of AuNPs was initially introduced in the pioneering work of Mühpfordt in 1982. This method was further refined by Slot and Geuze in 1985 as an effective means to produce smaller AuNPs compared to those obtained through the standard Turkevich method [40,41]. In summary, the AuNPs were made by adding $HAuCl_4$ (25 mM) to SC and TA in a mixed solution at 70 °C. As a result, the solution changed immediately after the injection of the gold precursor from transparent to dark gray, and subsequently, it turned brownish-orange within a short period, indicating the creation of very small AuNPs. For the creation of these tiny particles, the usage of traces of TA, which has a stronger reducing capacity than SC, appeared to be essential. However, the need for both reducing agents was necessary, as the absence of them led to the formation of large,

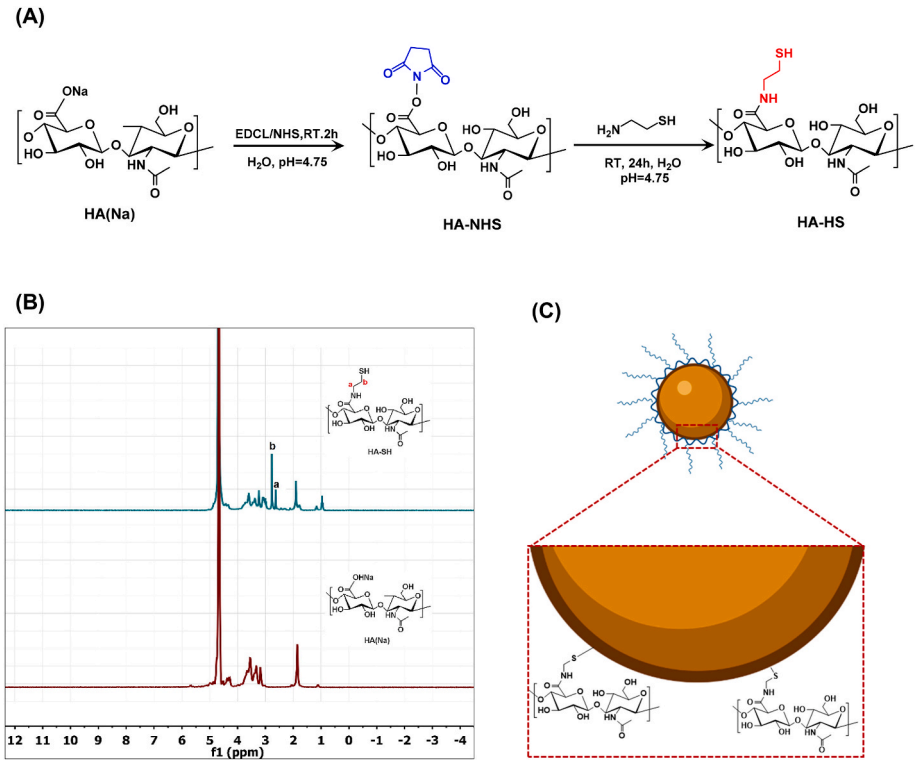

Scheme 1. Synthetic scheme for the fabrication of HA-SH functionalized AuNPs complexes (HA-SH/AuNPs). Synthetic process of: (A) Thiolated Hyaluronic Acid (HA-SH) (B); ^{1}H NMR (D_2O) spectra of HA and HA-SH (Mw 10 Da); (C) Schematic diagram of AuNPs surface passivated with HA-SH.

rather polydisperse-sized particles. To enhance the properties of AuNPs, they underwent a chemical modification process using HA-SH through a gold-thiol chemical reaction [42,43]. Coating of AuNPs with HA-SH is a valuable approach to enhance their properties and tailor them for specific applications, particularly in the fields of nanomedicine. The HA-SH coating improves biocompatibility, stability, water solubility and reduced immune response. In order to have pure HA-SH polymer, the remaining unbound HA-SH was removed by centrifugation and resuspension three times. The successful formation of HA-SH/AuNPs complex was confirmed by TEM, DLS, XRD, UV-VIS spectroscopy, and FT-IR spectral data analysis as described in the following section.

TEM morphological characterization of AuNPs and HA-SH/AuNPs shows the faceted nature of the synthesized particles along with its high monodispersity (Fig. 1A(a,d)). The statistical analysis of TEM images (Fig. 1A(b,e)) revealed that spherical AuNPs and HA-SH/AuNPs with the average size of 2.82 ± 1.77 nm, 6.56 ± 1.86 nm respectively and narrow size distribution (coefficient of variation about %15) were obtained in this method. The size distribution profiles obtained from DLS measurements for both AuNPs and HA-SH/AuNPs were quite similar, with average sizes of approximately 6.82 ± 1.79 nm for AuNPs and 12.56 ± 1.65 nm for HA-SH/AuNPs (Fig. 1A(c,f)). However, when we analyzed the size distribution of AuNPs created at 70 °C with the SC to $HAuCl_4$ molar ratio of 0.088, we found that the size distribution determined by DLS was broader than that observed using TEM. Nonetheless, it's important to note that there is a meaningful correlation between the two measurement methods [37]. The UV-VIS spectra obtained after adding $HAuCl_4$ to the solution offer important insights into the development of AuNPs. The initial spectrum exhibits a distinctive absorption maximum at 517 nm, indicating the presence of small-sized AuNPs in the solution. The confirmation of the effective modification of the AuNPs with HA-SH is evident from the change in the absorption peak, shifting from 517 nm to 523 nm as observed in the UV-VIS spectra. This indicates that the HA-SH has adsorbed onto the surface of the AuNPs and altered their local environment, without causing significant aggregation (Fig. 1B(a)). The crystalline nature of as-prepared lyophilized AuNPs and HA-SH/AuNPs was confirmed using XRD (Fig. 1B(b)). The XRD spectrum shows two predominant peaks at 40.36 and 66.28 that agree with AuNPs reported in previous literature [44]. On the other hand, no diffraction peaks in HA-SH, indicate the amorphous nature of the polymer. The diffraction peak of the AuNPs vanished in the HA-SH/AuNPs, indicating that the homogeneous HA-SH coating on the AuNPs caused the crystalline structure of the AuNPs to be broken by H-bonding and physical adsorption. Therefore, the lack of the HA-SH/AuNPs' distinctive diffraction peak suggested that there was no direct Au–Au packing mode in the HA-SH/AuNPs; instead, it was completely exfoliated and amorphous in nature, leading to the formation of a distinctive nanoparticle structure. To enable a qualitative analysis of the functional groups, present on HA-SH/AuNPs the chemical structures were confirmed by FT-IR (Fig. 1C(a)). FT-IR spectra provide structural and conformational information on citrates capping AuNPs after purification. The carboxylate asymmetric stretching band COO^- of AuNPs appeared at 1638 cm^{-1}. HA shows a peak at 1602 cm^{-1} associated with C=O stretching of carboxylate anion. The strong absorption at 1410 cm^{-1} and 1036 cm^{-1}, is assigned to carboxylate symmetric stretching and C–O–C stretching vibration of HA skeleton. The introduction of thiol groups in HA-SH can be identified by a distinct peak around 2770 cm^{-1} and a peak at 1558 cm^{-1} associated with C=O stretching of carboxylate amid groups. This peak corresponds to the stretching vibrations of the sulfur-hydrogen bonds. Furthermore, in the case of HA-SH/AuNPs, there are distinctive peaks at 1036 cm^{-1} and 2770 cm^{-1}, corresponding to the symmetric stretching of carboxylate groups and the stretching vibration of C–O bonds, indicative of the presence of thiol groups from HA-SH. Additionally, there's a peak at 1589 cm^{-1} associated with AuNPs, likely resulting from hydrogen bonds formed between the citrates on the AuNPs and OH groups in HA-SH chains. Notably, the peak at 3282 cm^{-1} has also shown a decrease in intensity. The strong association caused by the non-covalent interactions is the driving force for the direct coating of the HA-SH segments onto the AuNPs. Zeta potentials of AuNPs polymer conjugates provide important information on surface charge that is critical for many applications such

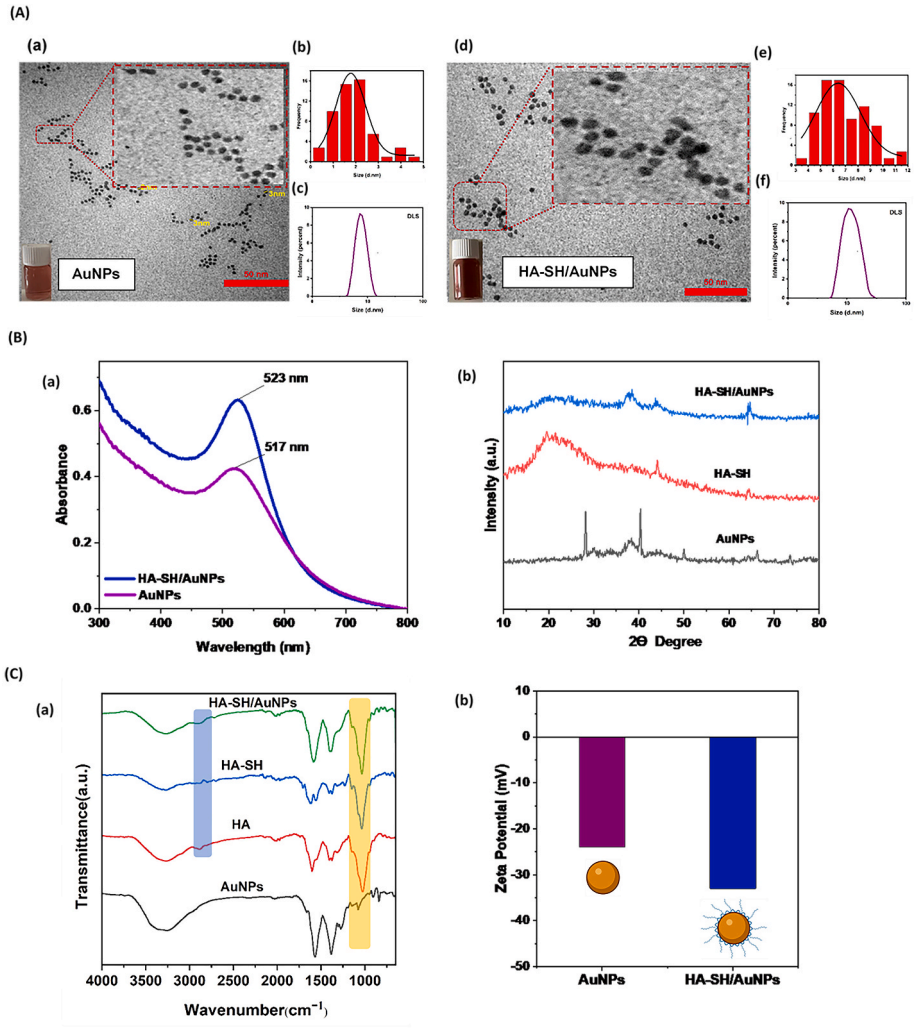

Fig. 1. (A) (a) Representative TEM images of AuNPs synthesized by injecting 1 mL of $HAuCl_4$ (25 mM) to a 150 mL solution of the combination of both SC and TA; (b) Size distribution analyzed from TEM images of AuNPs; (c) Size distribution profiles measured by DLS of AuNPs; (d) Representative TEM images of HA-SH/AuNPsc; (e) Size distribution analyzed from TEM images of HA SH/AuNPs; (f) Size distribution profiles measured by DLS of HA-SH/AuNPs. (B) (a) Absorbance spectra of AuNPs and HA-SH/AuNPs dispersed in water; (b) XRD spectra of AuNPs, HA-SH/AuNPs and HA-SH. (C) (a) FT-IR spectra of AuNPs, HA-SH/AuNPs, HA, and HA-SH; (b) Zeta potential of AuNPs and HA-SH/AuNPs.

as drug delivery. By studying the zeta potentials of nanosystems, the surface charge of bare AuNPs and HA-SH/AuNPs were compared (Fig. 1C(b)). The surface charge of HA-SH/AuNPs was highly negative due to the presence of HA (−33 mV). The AuNPs initially carried a negative charge due to the presence of citrate agents capping the nanoparticle surface, indicated by a zeta potential of −23 mV. However, following the introduction of negatively charged HA-SH chains, a coating formed on the nanoparticles, resulting in a significantly more negative surface charge, as evidenced by the zeta potentials spectrum of HA-SH/AuNPs.

3.2. Bench-scale production of 5-FU loaded cationic liposome formulations with microfluidic and thin film method

Similar to numerous liposome formulations, the cationic liposome (SPC/DOPE/DOTAP) is often prepared in the laboratory using the thin film method. However, this method is challenging to scale up and tends to result in high batch-to-batch variability. On the contrary, controllable technologies, such as microfluidics, provide a robust, continuous, and scale-independent production method. Hence, in this study, we have developed a microfluidic production technique for delivering 5-FU using cationic liposomes. This method is not contingent on the scale and yields liposomal systems with a comparable biodistribution to those generated through the small-scale thin film method. To identify the operating conditions that would yield liposomes with the highest lipid concentration and productivity, the hydrodynamic focusing technique employing a toroidal mixer design was employed. This design provides comparable mixing efficiencies under laminar flow at high fluid speeds by incorporating circular structures within the flow path. This induces chaotic advection by increasing the number of vortices and centrifugal forces created between the columns within the cartridge. This allows for enhanced mixing and enables higher throughput [45]. In this study, we have examined the physicochemical attributes of cationic liposomes loaded with 5-FU, formulated with SPC/DOPE/DOTAP, using both microfluidic and thin film methods with identical compositions (Fig. 2).

In the case of the microfluidic process, a pre-formulation study was carried out to set-up the operative conditions to generate liposomes of approximately 100 nm diameter. Small unilamellar liposomes can be rapidly formed within milliseconds in the toroidal mixer channels. This is attributed to the increase in polarity, which facilitates a nano-precipitation reaction, followed by supersaturation and self-assembly of lipid molecules [46]. Crucially, the microfluidic-based formulation significantly influences key physicochemical properties of liposomes, such as size and PDI, with considerable dependence on the flow rate

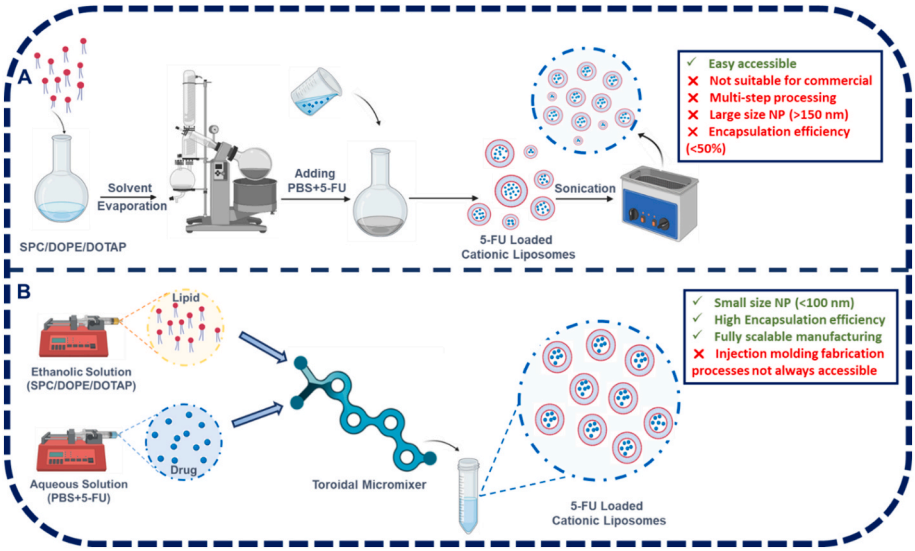

Fig. 2. 5-FU loaded cationic liposomes (SPC/DOPE/DOTAP) prepared using (A) the thin-film method and (B) the microfluidic system.

settings. Therefore, optimizing the entire process becomes challenging and time-consuming when employing a one-factor-at-a-time method. DoE plays a pivotal role in scientific inquiry by offering a systematic framework for planning, executing, and analyzing experiments. Its importance lies in its ability to provide researchers with a structured approach to investigate multiple variables simultaneously, enabling them to efficiently explore the complex interactions between these variables. By strategically designing experiments to manipulate and control variables, researchers can identify the key factors that influence the observed outcomes, optimize experimental conditions, and gain valuable insights into the underlying mechanisms of the studied phenomena.

For to determination of various processing parameters affected vesicle size and dispersion, the Taguchi method aims to optimize the desired outcomes by minimizing the influence of extraneous factors, thereby enhancing overall performance. The chosen design was instrumental in identifying specific factors and their interactions that would yield the highest response. The objective was to uncover conditions that would lead to the production of favorable end products. A conventional orthogonal array design, especially L_9, was used to carry out the screening experiment. This design structure was subsequently subjected to analysis using the Minitab software to identify the factors that held significant importance.

The DoE design space outlined here is derived from nine different runs with systematic variations in LR, TLC, FRR, and TFR, as detailed in Table 2. This strategy offers the possibility to assess the effect of these four items, LR (50:25:25, 55:25:20, and 55:20:25), TLC (5, 10, and 20 mM), FRR (from 1:1 to 1:5), and TFR (5–20 mL/min) on physicochemical characteristics of liposomes (particle size and PDI) using a minimal number of runs. To find the best design of experiments to achieve the minimum PDI, the signal-to-noise ratio plot was presented in Fig. 3. As discussed in Table 2, formulation 10 was found to demonstrate desired PDI (0.032 ± 0.0021) and particle size (75 ± 0.68 nm). For further experiments, the optimized formula (formulation 10) was used.

Contour plots use fitted response values related to two continuous variables based on a model equation (Fig. 4). A contour plot offers a two-dimensional representation in which all points with the same response are connected, forming contour lines that represent constant responses. Contour plots are beneficial for identifying favorable response values and determining optimal operating conditions. The results indicate that higher doses of TLC lead to a decrease in PDI and do not have a significant effect on particle size. As the TFR and FRR to LR increase, both particle size and PDI decrease to lower values. Finally, the relationship

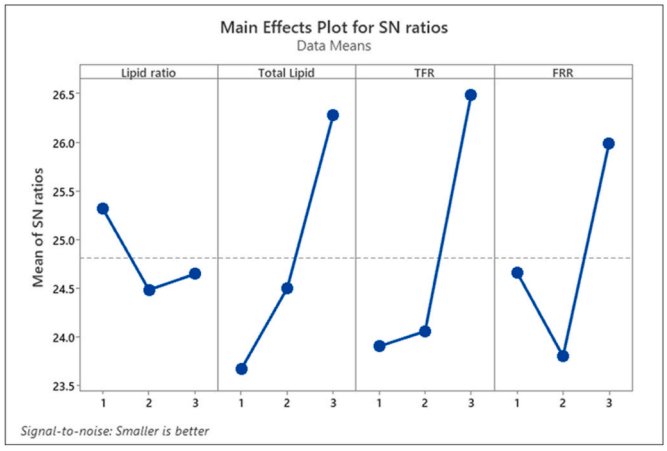

Fig. 3. The main effect of each factor reflected by signal-to-noise ratio curves.

between FRR and TFR was examined using 2D contour plots (Fig. 4). Interestingly, when the FRR was changed to larger numbers, liposome size decreased and the same result was found for TFR affecting the PDI of liposome particles.

3.2.1. *Physicochemical characteristics of 5-FU loaded cationic liposome*

5-FU was used as a model drug and was added into PBS solution to produce 5-FU loaded liposomes. This process was carried out using both the thin-film and a microfluidic method. In general, the EE is less than 10 % for passive loading of hydrophilic drugs [47]. Joshi et al. [48] showed that the loading of hydrophilic metformin is increased up to 20 % in a staggered herringbone micromixer (SHM) device. This enhancement can be attributed to the capability of microfluidic devices to improve the passive encapsulation efficiency of hydrophilic drugs. John et al. also [49] confirmed that the single flow-focusing device achieves a high efficiency for loading a hydrophilic tracer into the liposome.

In the microfluidic process, to validate our DoE-based formulation strategy, we used the flow rate settings identified during the DoE to incorporate 5-FU into liposomes with a defined hydrophilic characteristic of the drug (Fig. 5A). As measured by DLS, the 5-FU loaded cationic liposome produced by the microfluidic method showed uniform size distribution with a mean diameter of ~89.1 nm (Fig. 5B). Under TEM,

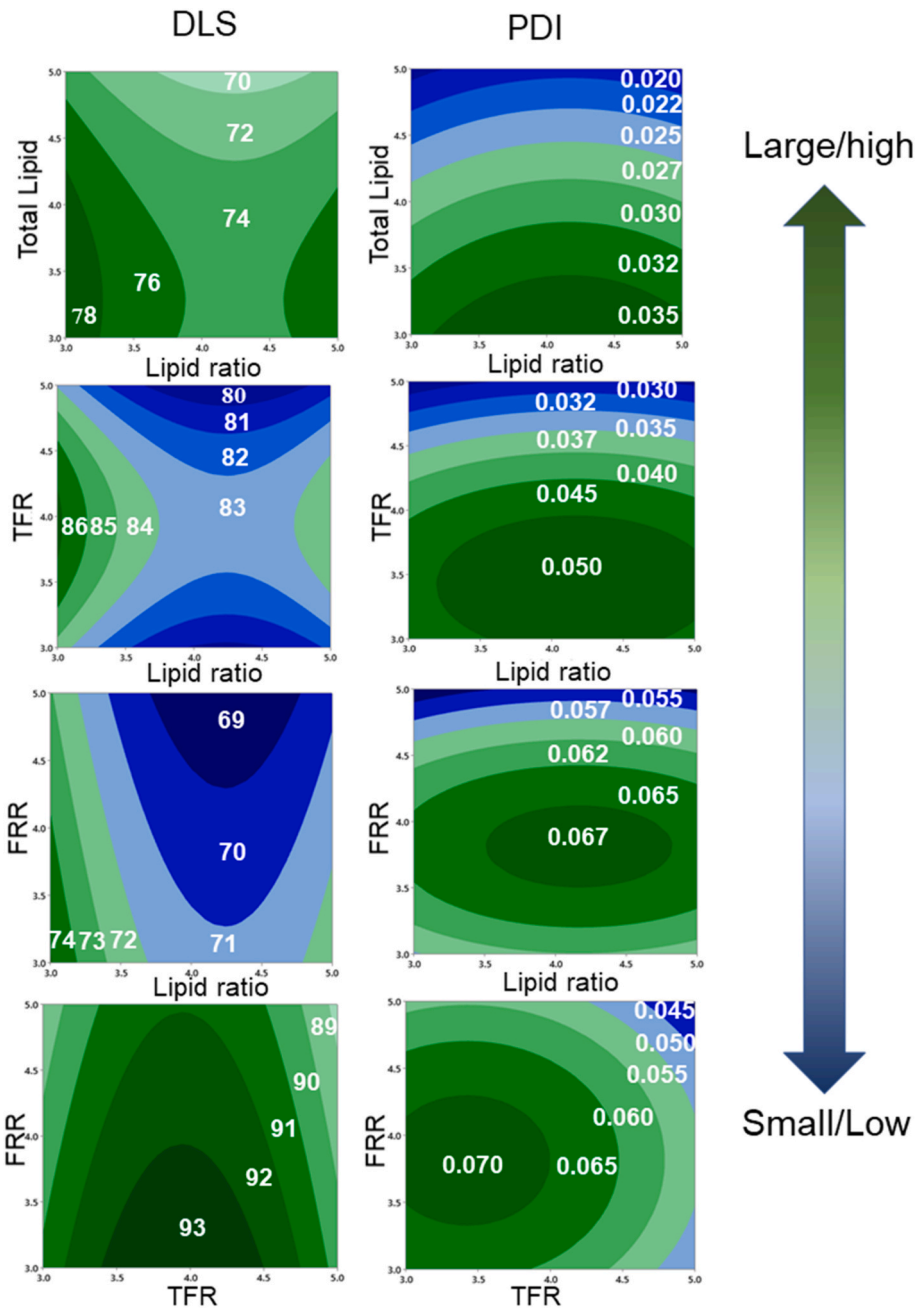

Fig. 4. DoE-based microfluidic optimization of therapeutic liposome formulations was done to evaluate their impact on the hydrodynamic size and size distribution (PDI) of the resultant liposomes, TFR, FRR, LR, and TLC was changed. DoE-based prediction models are displayed as two-dimensional contour plots with color codes that represent the sizes of the liposomes, ranging from small to large, and PDI values, which range from low to high. Specific dimensions and PDI values are displayed. The plots were constructed using Minitab software. (For interpretation of the references to color in this figure legend, the reader is referred to the Web version of this article.)

the obtained 5-FU loaded liposome showed flower-like morphology (staining agents such as uranyl acetate were used to the TEM samples before plunging in the grid) (Fig. 5C). The FE-SEM images before and after freeze-dry (Fig. 5D and E) were a further confirm to the successful role of microfluidic method in preparing nano-cationic liposomes loaded with 5-FU.

Following optimization of the microfluidic method, cationic liposomes (formulation 10) were produced using the thin film method as well as microfluidics, and the EE%, DL%, size distribution, and zeta potential were measured (Table 3). According to Table 3, the EE and DL of 5-FU through passive loading in liposomes produced with the microfluidic system were relatively high. This suggests the effective performance of this device in enhancing the encapsulation efficiency of hydrophilic drugs, making it adequate for the release of a therapeutic dose of the drug. Liposomes prepared using the thin-film method, as expected, reported a low EE (approx. <30 %) and the DL threshold was only 3.1 %. Of note, the concentration of 5-FU used in the microfluidic method and the thin-film preparation method is the same. It's crucial to highlight that there wasn't a substantial distinction in the initial lipid concentration employed in the two preparation techniques, with both thin-film and microfluidic liposome formulations starting at 5.98 mg/mL of lipid. This influenced the ultimate concentration of encapsulated 5-FU, as the formulations were intended to maintain a consistent 5-FU to lipid ratio (1:0.38 for both thin-film and microfluidic formulations).

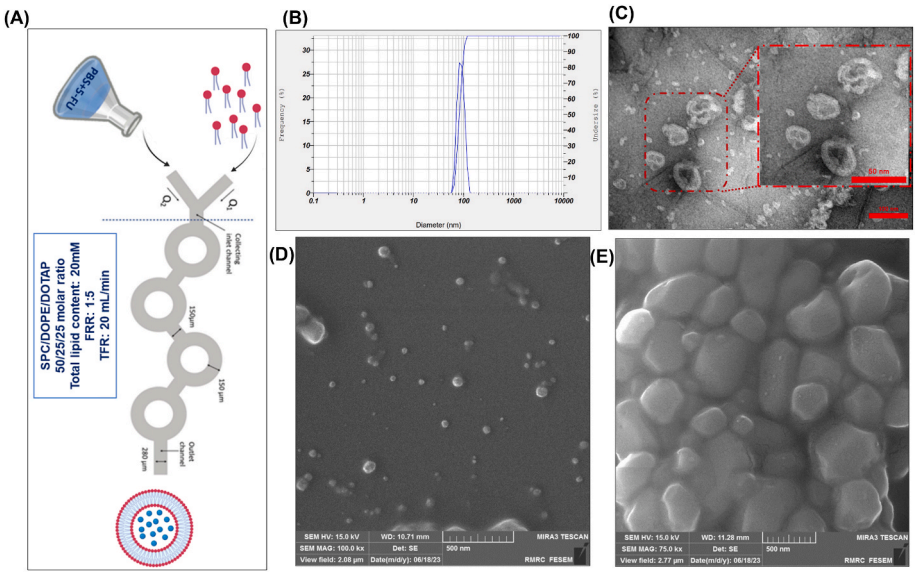

Fig. 5. Validation and characterization of DoE prediction model (formulation 10). (A) Schematic representation of microfluidics-based encapsulation of hydrophilic drug (5-FU) into a clinical liposome formulation (Toroidal micromixer adapted from Belliveau et al. [50]). (B) DLS size distributions of cationic liposome. (C) TEM micrograph of free cationic liposomes. (D), (E) FE-SEM micrograph of free cationic liposomes before and after freeze dry respectively.

Table 3
Physicochemical properties of the 5-FU loaded cationic liposomes that produced with thin film and microfluidic method (Data are presented as mean ± st.dev. of n = 3 independent formulations, each result is the mean of N = 3 measurements).

Formation Method	Encapsulation Efficiency (%)	Drug Loading (%)	Size Distribution				Zeta Potential (mV)
			Z-Average (nm)	PDI	Peak 1 Intensity (nm)	Peak 1 Volume (nm)	
Microfluidic method	65.87 ± 1.20	31.1 ± 0.3	90.22	0.032 ± 0.0021	89.1 ± 0.78 (100 %)	74.45 ± 0.94 (100 %)	+21.1 ± 2.3
Thin film method	27.35 ± 2.51	3.1 ± 2.9	193.7	0.52 ± 0.083	184.1 ± 23.7 (54.8 %)	190.1 ± 5.13 (66.9 %)	+24.39 ± 2.05

Concerning the microfluidics preparation, liposomes that passively encapsulated 5-FU demonstrated levels of EE of 65.87 ± 1.20 %, and DL above 31.1 ± 0.3 %. Overall, the microfluidic method tends to offer advantages in terms of both EE and DL, particularly for hydrophilic drugs. This is due to the superior mixing and encapsulation capabilities provided by microfluidic devices.

As depicted in Table 3, achieving a narrow size distribution for liposomes produced using the thin film method can be a challenging task (PDI: 0.52 ± 0.083). This is because the process involves rehydrating a dried lipid film, which can lead to a wider range of liposome sizes. The resulting liposomes may vary in diameter, leading to a broader size distribution. The liposomes produced through the microfluidic method exhibit a narrower PDI (0.032 ± 0.0021), resulting in uniform and smaller particle sizes. In the context of the thin film and microfluidic method, z-average typically refers to the average or mean size of liposomes formed during the preparation process. In the microfluidic method, z-average often signifies a more precise and uniform liposome size. Microfluidic devices are known for their ability to produce liposomes with a narrow and well-defined size distribution. Consequently, the z-average obtained in the microfluidic method (z-average: 90.22 nm) tends to be more consistent, with liposomes closely clustered around a single-size value. According to one study, the zeta potential of 5-FU loaded liposomes prepared by the thin film method was +24.39 ± 2.05 mV, while the zeta potential of liposomes prepared by the microfluidic method was +21.1 ± 2.3 mV. This suggests that the microfluidic method produces liposomes with less positive charge than the thin film method, which may affect their stability. Zeta potential can affect the stability, aggregation, and interaction of liposomes with other molecules. In summary, liposomes generated through the microfluidic technique tend to demonstrate superior characteristics when compared to those produced using the thin film method, particularly in terms of z-average size and PDI. The microfluidic approach generally results in liposomes with a more consistent size distribution (less variation in z-average size) and lower PDI, signifying a higher degree of uniformity in liposome size. For further experiments, the optimized formula (formulation 10) was used. Certainly, we proceeded with further analyses on the liposomes generated using the microfluidic method (formulation 10).

3.2.2. Preparation of HA-SH/AuNPs@Liposomes using post-microfluidics conjugation approach

The effectiveness of cationic liposomes is frequently hindered by their limited stability. A developing approach to enhance the stability of liposomes for effective drug delivery involves attaching small charged nanoparticles to the surfaces of liposomes. The nonspecific adsorption of these charged nanoparticles onto phospholipid bilayers creates steric repulsion, preventing liposomes from coming into proximity and subsequently inhibiting the fusion that would lead to the formation of larger vesicles [51]. The goal of this study is to create a distinctive and durable system of nanoparticle-stabilized liposomes using a post-microfluidics conjugation approach for the delivery of a chemotherapeutic drug. The specific focus is on delivering the antimetabolite 5-FU to treat NMSC. To achieve this objective, we present a well-established pH-responsive gold nanoparticle-stabilized liposome system in which small nanoparticles (HA-SH/AuNPs) (diameter ~12 nm) bind to the surface of cationic liposomes SPC/DOPE/DOTAP (50/25/25 M ratio) (diameter

~75 nm) that produced with microfluidic approach and thus stabilize the liposomes at neutral value (i.e., pH 7.4). These gold stabilizers will detach from the liposomes when the environmental acidity decreases to near acidic pH values (i.e., extracellular acidity in tumor tissue of head and neck squamous cell carcinoma) [52].

A stimuli-responsive system comprising gold nanoparticle-stabilized liposomes involves synthesizing positively charged liposomes and introducing negatively charged HA-SH/AuNPs that can be absorbed onto the liposome surface. When gold-stabilized liposomes encounter an acidic environment (pH 4, 5.5), these negatively charged nanoparticles undergo protonation. The HA-SH/AuNPs lose their charge and detach from the liposome's surface, thus restoring their ability to fuse [53].

The preparation of HA-SH/AuNPs@Liposomes, can be divided into three steps. First, HA-SH/AuNPs nanoparticles were synthesized as described in Section 2.5, where chemical reduction of the gold precursor $HAuCl_4$ by dissolved SC and then stabilized by adding HA in ambient conditions. The electrophoretic mobility measurements with DLS showed that the surface zeta potential of HA-SH/AuNPs was -33.4 ± 1.0 mV, a strong negative charge implying the presence of anionic carboxylate groups of HA on the particle surfaces. In the second step, liposomes consisting of SPC, DOPE, and DOTAP (in a weight ratio of 50:25:25) were prepared by using a microfluidic hydrodynamic flow focusing method. The surface zeta potential of bare Liposomes showed $+21.1 \pm 2.3$ mV (Fig. 6A). The significant positive zeta potential of bare liposomes confirms the integration of DOTAP into the lipid bilayers, especially when compared to liposomes formulated without DOTAP, which exhibited a similar size but a less positive zeta potential of 3.6 ± 0.4 mV. Lastly, the resulting anionic HA-SH/AuNPs nanoparticles and the cationic liposomes were mixed at a molar ratio of 30:1 under gentle bath sonication for 10 min. Following the preparation, DLS measurements showed that the HA-SH/AuNPs@Liposomes had a diameter of 102.2 ± 1.3 nm (PDI $= 0.11 \pm 0.01$) and a surface zeta potential of -19.7 ± 0.7 mV (Fig. 6A and B). Compared to bare liposomes, the observed approximate 30 nm diameter increase of particle size is likely due to the adsorption of HA-SH/AuNPs onto the liposome surfaces. The switch of zeta potential from 21.1 to −19.7 mV also confirms the binding of negatively charged HA-SH/AuNPs nanoparticles to the liposomes. The morphology and structure of the HA-SH/AuNPs@Liposomes were further imaged by TEM. As shown in Fig. 6C, individual HA-SH/AuNPs particles were visible on the surface of liposomes after they were deposited on a TEM grid.

As evident from the results, this innovative system employs a stimuli-responsive approach. It involves synthesizing positively charged liposomes and introducing negatively charged HA-SH/AuNPs to bind onto the liposome surface. Notably, the system exhibits pH-responsive behavior, where the gold stabilizers detach under acidic conditions. This leads to a significant shift in the zeta potential of the cationic liposomes to $+21.1 \pm 2.3$ mV. Importantly, these cationic liposomes interact efficiently with the negatively charged skin barrier, facilitating enhanced penetration through the skin.

3.2.3. *Controlled drug release and kinetics release model of 5-FU from cationic liposomes produced with microfluidic method*

In vitro, drug release profiles can be employed to understand the behavior pattern of drug release in vivo. The rate of drug release from liposomes is influenced by factors such as liposome composition and the composition of the entrapped drug [54]. The in vitro drug release performances of 5-FU loaded HA-SH/AuNPs@Liposomes were investigated by UV-VIS. The pH responsiveness of 5-FU release from liposomes were studied in the simulated physiological environment of normal tissues (pH 7.4) and acidic environment of tumors (pH 4 and 5.5), respectively. To validate the pH responsiveness of the nanoparticle-stabilized platform, the drug release from HA-SH/AuNPs@Liposomes was investigated in different pH environments over 10 days. As depicted in Fig. 7A, the 5-FU/liposome platforms with HA-SH/AuNPs attachments demonstrated stability in a neutral pH environment (pH 7.4) and presented

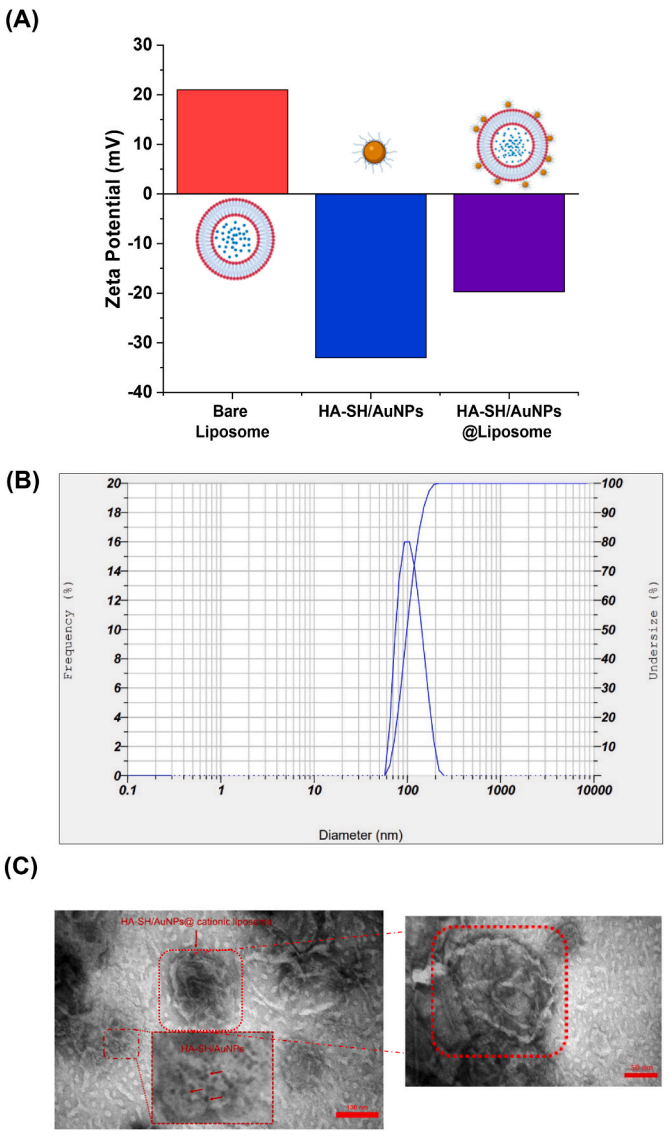

Fig. 6. (A) A comparison study of bare liposomes, HA-SH/AuNPs and HA-SH/AuNPs@cationic liposomes were carried out to measure zeta potential. (B) DLS size distributions of HA-SH/AuNPs@cationic liposomes. (C) TEM micrograph of HA-SH/AuNPs@Liposomes.

minimal release. However, when HA-SH/AuNPs@Liposomes were exposed to an acidic environment, they exhibited a 75.85 % and 70.81 % drug release over 7 days at pH 4 and pH 5.5, respectively. This pH-responsive system demonstrates versatile and effective drug release profiles across different pH conditions. At pH 7.4, the system maintains controlled and gradual drug release, suitable for healthy skin and normal cells. At pH 5.5, the system shows enhanced drug release, aligning with the acidic microenvironment of melanoma cells, making it effective for targeting melanoma specifically. At pH 4, the system exhibits rapid drug release, ideal for treating conditions with highly acidic environments such as severe infections and aggressive tumors.

Furthermore, the drug release pattern closely resembled that of bare liposomes. As a control, bare liposomes were subjected to various pH conditions, but no significant difference in drug release was observed. The notable contrast in drug release activity suggests that HA-SH/AuNPs@Liposomes are pH-responsive. In a neutral pH environment, the liposome stabilization was maintained, preventing premature leakage of 5-FU from the liposomes (Fig. 7A). As a result, this platform design achieves two objectives. The first is to create steric repulsion, preventing fusion with other neighboring liposomes. The second is to

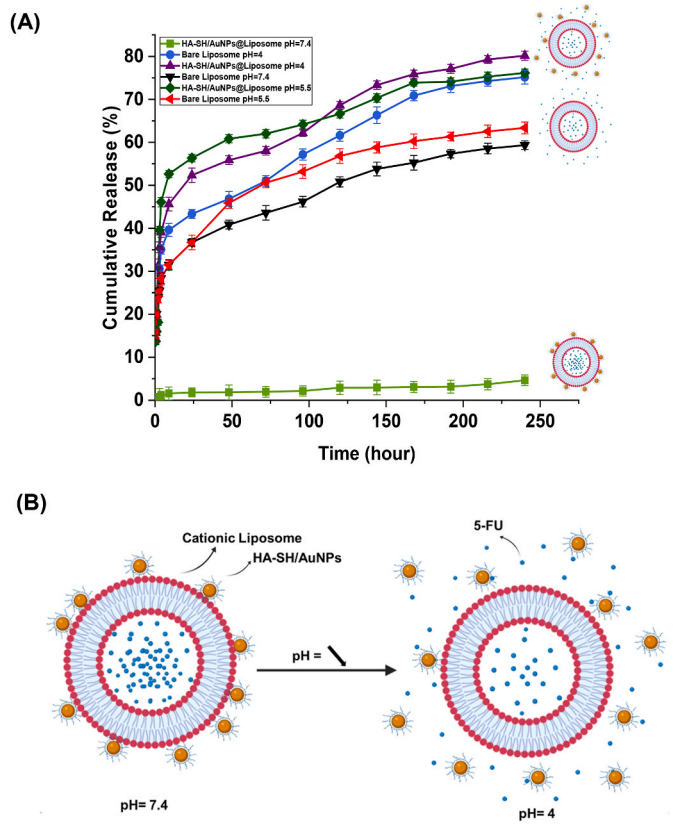

Fig. 7. (A) 5-FU release study based on varying pH environments. Only when HA-SH/AuNPs@Liposomes were placed in an acidic environment, did the liposomes exhibit the same drug release activity as bare liposomes. The drug release of bare liposomes showed no difference despite the change in the pH environment. (B) The schematic of the pH-responsive liposome platform. In a neutral pH environment (pH 7.4), HA-SH/AuNPs absorb to the liposome's surface, stabilizing the liposome, and preventing inner drug molecules from being released. Once liposomes are placed in an acidic environment (pH 4), HA-SH/AuNPs particles lose their negative charge and detach from the liposome surface, enabling liposomes to regain their fusion capability and release their drug cargo.

stabilize liposomes, thereby preventing drug leakage. As shown in Fig. 7B, HA-SH/AuNPs persist attached to liposomes when placed in a neutral pH environment (pH 7.4). However, when these nanoparticle-stabilized liposomes are exposed to an acidic environment, the HA-SH/AuNPs will detach from the liposome surface. This allows the liposomes to freely release the drug.

3.2.4. Stability

The stability of liposomes plays a crucial role in maintaining the integrity and functionality of liposomal formulations. The physical stability of liposomes is evaluated by size change (aggregation) and surface charge (zeta potential). Zeta potential is an indicator of colloidal stability of particles which is higher when particle charge is sufficiently high for them to repel each other, and a higher absolute value of zeta potential indicates higher stability [55]. To investigate the physical stability, bare liposome, and HA-SH/AuNPs@Liposome formulations prepared in this study were stored at 4 °C and 37 °C immediately after fabrication. The z-average size, PDI, and zeta potential were assessed at multiple times over 4-weeks (Table 4). Both bare liposomes and HA-SH/AuNPs@Liposomes exhibited a slight size increase over 4 weeks at 4 °C, compared to the size increase observed at 37 °C. The DLS analysis revealed that the HA-SH/AuNPs@Liposomes stored at 4 °C exhibited a slight increase in particle size, changing from 102.2 ± 1.3 to 107.54 ± 0.43. In contrast, the bare liposomes experienced a more substantial size increase under the same storage conditions, going from 90.22 ± 0.69 to 129.45 ± 0.89. The information presented in Table 4 indicates that under storage conditions at 37 °C, the bare liposomes underwent a significant enlargement in particle size, escalating from 90.22 ± 0.69 to 190.89 ± 0.65 nm. In contrast, the HA-SH/AuNPs@Liposomes exhibited a more modest increase in size under the same temperature conditions (102.2 ± 1.3 to 116.76 ± 0.26). The data regarding the PDI showed a similar trend to the particle size findings. Notably, the group of HA-SH/AuNPs@Liposomes stored at 4 °C demonstrated the least PDI alteration, indicating greater uniformity in particle size distribution. The zeta potential results show negligible changes, particularly at a temperature of 4 °C. After storage, the zeta potential values of HA-SH/AuNPs@Liposomes increased slightly (−19.7 ± 0.7 to −22.9 ± 0.8 mV). Commonly, the samples having higher zeta potential do not aggregate as a result of electric repulsion [56]. These findings suggest that the incorporation of AuNPs into liposomes enhances their long-term stability in comparison to liposomes without any added content.

3.3. In vitro biocompatibility and antitumor efficacy

The in vitro biocompatibility of free liposomes (The concentration range tested was between 1 and 30 (mM)), HA-SH, AuNPs, HA-SH/AuNPs, and HA-SH/AuNPs@Liposomes on normal HaCaT was evaluated using MTT assay and the result showed no significant cytotoxicity in comparison with control (Fig. 8).

As depicted in Fig. 8 (A), at doses ranging from 1 to 30 mM, the free liposomes demonstrated minimal cytotoxicity towards the cells, maintaining cell viability above 80 %. This suggests that these innovative liposomes exhibit low toxicity, making them a promising candidate for an effective drug delivery system. Notably, the cytocompatibility results for the final system, utilizing a concentration of 20 mM, revealed approximately 84 % cell viability after 3 days, further indicating the favorable biocompatibility of the liposomal formulation. The results also indicate that the HA-SH, AuNPs, HA-SH/AuNPs, and HA-SH/

Table 4
Physical stability of bare liposomes and HA-SH/AuNPs@Liposomes after preparation and storage (4 weeks, 4 °C and 37 °C). Of note, samples were not filtered after production and before measurements. Data are presented as mean ± st. dev. of n = 3 independent formulations, each result is the mean of N = 3 measurements.

Liposomal system	Z-average size (nm) as prepared	Z-average size (nm) after storage	PDI as prepared	PDI after storage	Z -potential (mV) as prepared	Z -potential (mV) after storage
Bare liposome Storage at 4°C	90.22 ± 0.69	129.45 ± 0.89	0.032 ± 0.02	0.042 ± 0.05	21.1 ± 2.3	20.1 ± 1.3
Bare liposome Storage at 37°C		190.89 ± 0.65		0.071 ± 0.01		14.1 ± 3.2
HA-SH/ AuNPs@Liposomes Storage at 4°C	102.2 ± 1.3	107.54 ± 0.43	0.11 ± 0.01	0.19 ± 0.03	−19.7 ± 0.7	−22.9 ± 0.8
HA-SH/ AuNPs@Liposomes Storage at 37°C		116.76 ± 0.26		0.21 ± 0.01		−16.7 ± 0.9

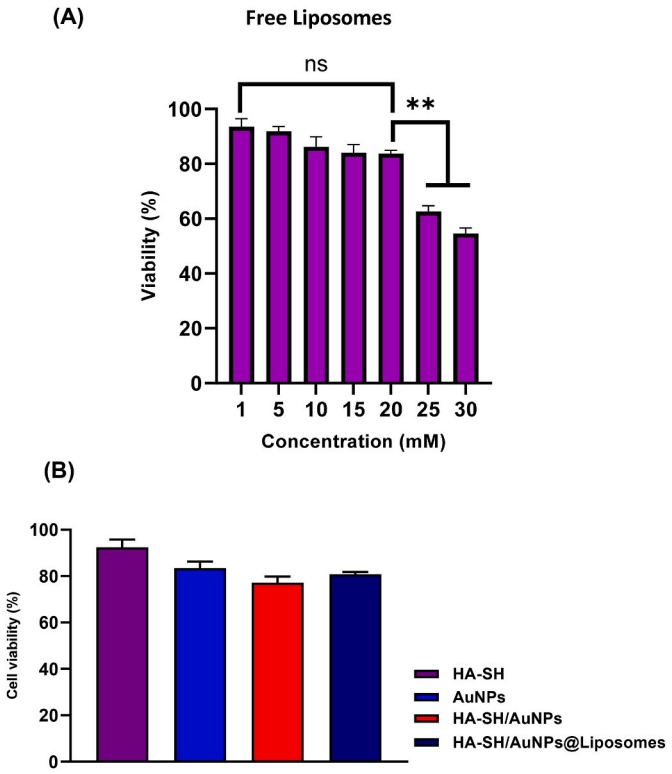

Fig. 8. Biocompatibility evaluation by MTT assay on HaCaT cell line using different samples as shown (mean ± SD, n = 3), (A) after incubation with free liposome solution (in 1–30 mM concentration), (B) HA-SH, AuNPs, HA-SH/AuNPs, and HA-SH/AuNPs@Liposomes.

AuNPs@Liposomes groups exhibit relatively good cytocompatibility, with approximately 92 %, 83 %, 77 %, and 80 % cell viability after 3 days, respectively.

The MTT assay was also conducted to evaluate the potential cytotoxic effect of drug-loaded HA-SH/AuNPs@Liposomes on skin cancer A431 skin carcinoma cells viability. The cell viability profiles after culturing for 3 days in DMEM medium containing free 5-FU, free HA-SH/AuNPs@Liposomes, and drug-loaded HA-SH/AuNPs@Liposomes (5-FU, 1 mg. mL^{-1}) are shown in Fig. 9. As depicted in Fig. 9, both the free drug (5-FU) and the drug-loaded liposomes exhibited considerable cytotoxicity against A431 cells. Treatment with both the free drug and the 5-FU_HA-SH/AuNPs@Liposomes system significantly reduced the viability of A431 cells. Notably, there was no significant difference in cellular toxicity between the free 5-FU (approximately 86 % viability) and 5-FU_HA-SH/AuNPs@Liposomes (approximately 83 % viability) 72 h post-incubation. The blank HA-SH/AuNPs@Liposomes displayed low cellular toxicity on A431 cells, with approximately 89 % cell viability. Consequently, the 5-FU_HA-SH/AuNPs@Liposomes system demonstrated a significant synergistic reduction in cell growth and viability in A431 cells.

4. Conclusions

Hybrid liposome/metal nanoparticles stand out as promising contenders for nanomedicine applications. The primary objective of this article is to formulate a robust hybrid system capable of encapsulating the anticancer drug 5-FU, with the specific aim of treating NMSC and tailored for topical administration. This paper first compares cationic liposomal formulations (SPC/DOPE/DOTAP) prepared using a toroidal microfluidic mixer system with those made through the conventional thin-film hydration approach. Liposomes created with the microfluidic system were found to be comparable in size, surface charge, stability,

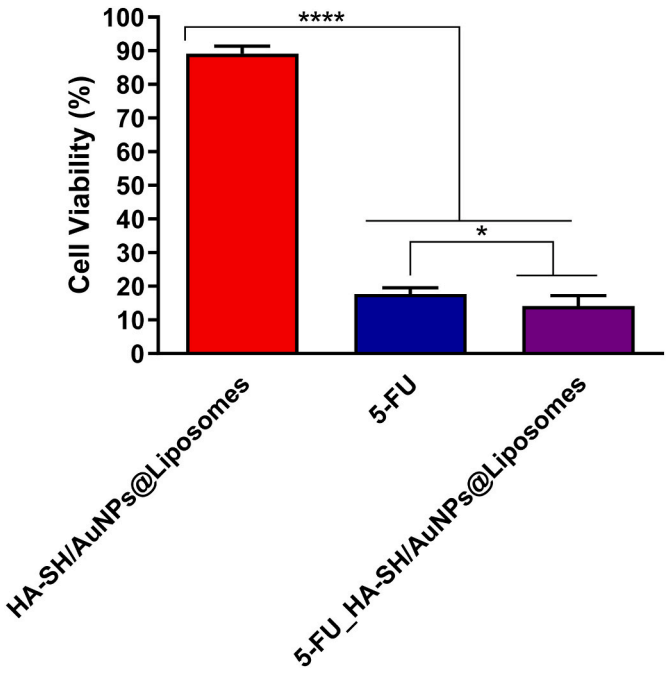

Fig. 9. Cytotoxicity evaluation by MTT assay on A431 cell line using different samples as shown (mean ± SD, n = 3), after incubation with free HA-SH/AuNPs@Liposomes solution, 5-FU, and 5-FU_HA-SH/AuNPs@Liposomes.

and drug loading capacity to those from the thin-film method. In the next step, we utilized the cationic liposomes produced via the microfluidic method to create a liposomal system (HA-SH/AuNPs@liposomes) with a zeta potential of −19.7 ± 0.7 mV. This innovative system employs a stimuli-responsive approach, where positively charged liposomes are synthesized and HA-SH/AuNPs, which are negatively charged, are introduced to bind onto the liposome surface. Notably, the system exhibits pH-responsive behavior, as the gold stabilizers detach in acidic conditions, resulting in a shift in the cationic liposomes' zeta potential to +21.1 ± 2.3 mV. This unique feature makes the system particularly suitable for topical applications, such as in the form of a liposomal ointment, targeting skin diseases characterized by acidic tissue environments, such as the extracellular acidity observed in head and neck squamous cell carcinoma tumor tissue. The studies indicated that cationic liposomes exhibited low cytotoxicity on the HaCaT cell line, suggesting their biocompatibility. In contrast, 5-FU_HA-SH/AuNPs@Liposomes demonstrated high cytotoxicity against the A431 cancer cell line. In conclusion, nanoparticle-stabilized cationic liposomes with acid-responsive stability and non-fusion activity were formed by attaching HA-SH/AuNPs to the outer surface of cationic liposomes. In summary, our objective is to lay the groundwork for the potential utilization of HA-SH/AuNPs@Liposomes in the form of liposomal ointments holds significant promise for advancing localized drug delivery systems in skin cancer treatment. The unique combination of enhanced penetration, sustained release, and targeted therapy positions this approach as a valuable and potentially transformative option for optimizing therapeutic outcomes in dermatological applications. This innovative approach has the potential to introduce a new era of liposomal applications.

Associated content

No Supporting Information.

Funding sources

No funding to declare.

CRediT authorship contribution statement

Sarvenaz Pakian: Writing – review & editing, Writing – original draft, Project administration, Methodology, Formal analysis, Data curation, Conceptualization. **Ahmad Mirkani:** Software. **Hamid Sadeghi-Abandansari:** Writing – review & editing. **Mohammad-reza Nabid:** Project administration, Funding acquisition.

Declaration of competing interest

The authors declare that they have no known competing financial interests or personal relationships that could have appeared to influence the work reported in this paper.

Data availability

The data that has been used is confidential.

Acknowledgment

This work was supported by Shahid Beheshti University Research Council.

References

[1] O.S. Fenton, K.N. Olafson, P.S. Pillai, M.J. Mitchell, R. Langer, Advances in biomaterials for drug delivery, Adv. Mater. 30 (2018) 1705328.
[2] K. Osouli-Bostanabad, S. Puliga, D.R. Serrano, A. Bucchi, G. Halbert, A. Lalatsa, Microfluidic manufacture of lipid-based nanomedicines, Pharmaceutics 14 (2022) 1940.
[3] B. García-Pinel, C. Porras-Alcalá, A. Ortega-Rodríguez, F. Sarabia, J. Prados, C. Melguizo, J.M. López-Romero, Lipid-based nanoparticles: application and recent advances in cancer treatment, Nanomaterials 9 (2019) 638.
[4] R. Tenchov, R. Bird, A.E. Curtze, Q. Zhou, Lipid nanoparticles— from liposomes to mRNA vaccine delivery, a landscape of research diversity and advancement, ACS Nano 15 (2021) 16982–17015.
[5] N.D. Donahue, H. Acar, S. Wilhelm, Concepts of nanoparticle cellular uptake, intracellular trafficking, and kinetics in nanomedicine, Adv. Drug Deliv. Rev. 143 (2019) 68–96.
[6] T.M. Allen, P.R. Cullis, Liposomal drug delivery systems: from concept to clinical applications, Adv. Drug Deliv. Rev. 65 (2013) 36–48.
[7] T.A. Balbino, N.T. Aoki, A.A. Gasperini, C.L. Oliveira, A.R. Azzoni, L.P. Cavalcanti, L.G. de la Torre, Continuous flow production of cationic liposomes at high lipid concentration in microfluidic devices for gene delivery applications, Chem. Eng. J. 226 (2013) 423–433.
[8] H. Zhang, Thin-film hydration followed by extrusion method for liposome preparation, Liposomes, Methods and protocols (2017) 17–22.
[9] J. Wang, J. Gong, Z. Wei, Strategies for liposome drug delivery systems to improve tumor treatment efficacy, AAPS PharmSciTech 23 (2022) 1–14.
[10] V.V.S.N.L. Andra, S. Pammi, L.V.K.P. Bhatraju, L.K. Ruddaraju, A comprehensive review on novel liposomal methodologies, commercial formulations, clinical trials and patents, Bionanoscience 12 (2022) 274–291.
[11] S.A. Roberts, N. Parikh, R.J. Blower, N. Agrawal, SPIN: rapid synthesis, purification, and concentration of small drug-loaded liposomes, J. Liposome Res. 28 (2018) 331–340.
[12] X. Zhao, F. Bian, L. Sun, L. Cai, L. Li, Y. Zhao, Microfluidic generation of nanomaterials for biomedical applications, Small 16 (2020) 1901943.
[13] C.B. Roces, E.C. Port, N.N. Daskalakis, J.A. Watts, J.W. Aylott, G.W. Halbert, Y. Perrie, Rapid scale-up and production of active-loaded PEGylated liposomes, Int. J. Pharm. 586 (2020) 119566.
[14] A. Maged, R. Abdelbaset, A.A. Mahmoud, N.A. Elkasabgy, Merits and advances of microfluidics in the pharmaceutical field: design technologies and future prospects, Drug Deliv. 29 (2022) 1549–1570.
[15] S.J. Shepherd, D. Issadore, M.J. Mitchell, Microfluidic formulation of nanoparticles for biomedical applications, Biomaterials 274 (2021) 120826.
[16] A. Jahn, W.N. Vreeland, M. Gaitan, L.E. Locascio, Controlled vesicle self-assembly in microfluidic channels with hydrodynamic focusing, J. Am. Chem. Soc. 126 (2004) 2674–2675.
[17] A. Wild, T. Leaver, R.J. Taylor, Bifurcating Mixers and Methods of Their Use and Manufacture, Google Patents, 2018.
[18] C. Webb, N. Forbes, C.B. Roces, G. Anderluzzi, G. Lou, S. Abraham, L. Ingalls, K. Marshall, T.J. Leaver, J.A. Watts, Using microfluidics for scalable manufacturing of nanomedicines from bench to GMP: a case study using protein-loaded liposomes, Int. J. Pharm. 582 (2020) 119266.
[19] D. Pornpattananangkul, L. Zhang, S. Olson, S. Aryal, M. Obonyo, K. Vecchio, C.-M. Huang, L. Zhang, Bacterial toxin-triggered drug release from gold nanoparticle-stabilized liposomes for the treatment of bacterial infection, J. Am. Chem. Soc. 133 (2011) 4132–4139.
[20] L. Zhang, S. Granick, How to stabilize phospholipid liposomes (using nanoparticles), Nano Lett. 6 (2006) 694–698.
[21] R. Michel, T. Plostica, L. Abezgauz, D. Danino, M. Gradzielski, Control of the stability and structure of liposomes by means of nanoparticles, Soft Matter 9 (2013) 4167–4177.
[22] N. Elahi, M. Kamali, M.H. Baghersad, Recent biomedical applications of gold nanoparticles: a review, Talanta 184 (2018) 537–556.
[23] D. Pornpattananangkul, S. Olson, S. Aryal, M. Sartor, C.-M. Huang, K. Vecchio, L. Zhang, Stimuli-responsive liposome fusion mediated by gold nanoparticles, ACS Nano 4 (2010) 1935–1942.
[24] B.Y. Moghadam, W.-C. Hou, C. Corredor, P. Westerhoff, J.D. Posner, Role of nanoparticle surface functionality in the disruption of model cell membranes, Langmuir 28 (2012) 16318–16326.
[25] B.B. Karakocak, J. Liang, P. Biswas, N. Ravi, Hyaluronate coating enhances the delivery and biocompatibility of gold nanoparticles, Carbohydr. Polym. 186 (2018) 243–251.
[26] S. Streck, A.J. Clulow, H.M. Nielsen, T. Rades, B.J. Boyd, A. McDowell, The distribution of cell-penetrating peptides on polymeric nanoparticles prepared using microfluidics and elucidated with small angle X-ray scattering, J. Colloid Interface Sci. 555 (2019) 438–448.
[27] S. Streck, H. Neumann, H.M. Nielsen, T. Rades, A. McDowell, Comparison of bulk and microfluidics methods for the formulation of poly-lactic-co-glycolic acid (PLGA) nanoparticles modified with cell-penetrating peptides of different architectures, Int. J. Pharm. X 1 (2019) 100030.
[28] J. Piella, N.G. Bastus, V. Puntes, Size-controlled synthesis of sub-10-nanometer citrate-stabilized gold nanoparticles and related optical properties, Chem. Mater. 28 (2016) 1066–1075.
[29] S. Bian, M. He, J. Sui, H. Cai, Y. Sun, J. Liang, Y. Fan, X. Zhang, The self-crosslinking smart hyaluronic acid hydrogels as injectable three-dimensional scaffolds for cells culture, Colloids Surf. B Biointerfaces 140 (2016) 392–402.
[30] R. Terracciano, Y. Carcamo-Bahena, E.B. Butler, D. Demarchi, A. Grattoni, C. S. Filgueira, Hyaluronate-thiol passivation enhances gold nanoparticle peritumoral distribution when administered intratumorally in lung cancer, Biomedicines 9 (2021) 1561.
[31] H. Lee, M.-Y. Lee, S.H. Bhang, B.-S. Kim, Y.S. Kim, J.H. Ju, K.S. Kim, S.K. Hahn, Hyaluronate–gold nanoparticle/tocilizumab complex for the treatment of rheumatoid arthritis, ACS Nano 8 (2014) 4790–4798.
[32] A.D. Bangham, M.M. Standish, J.C. Watkins, Diffusion of univalent ions across the lamellae of swollen phospholipids, J. Mol. Biol. 13 (1965), 238-IN227.
[33] M. Tsakiri, A.G. Tabriz, N. Naziris, K. Rahali, D. Douroumis, C. Demetzos, Exosome-like genistein-loaded nanoparticles developed by thin-film hydration and 3D-printed Tesla microfluidic chip: a comparative study, Int. J. Pharm. 651 (2024) 123788.
[34] P.K. Soni, T.R. Saini, Purification of drug loaded liposomal formulations by a novel stirred cell ultrafiltration technique, Pharm. Nanotechnol. 9 (2021) 347–360.
[35] W. Cong, Q. Liu, X. Chen, R. Gao, J. Lu, Y. Wang, G. Luo, Characterization and pharmacokinetics of a novel pirarubicin liposome powder, Drug Dev. Ind. Pharm. 36 (2010) 1186–1194.
[36] K. Katharotiya, G. Shinde, D. Katharotiya, S. Shelke, R. Patel, D. Kulkarni, P. Panzade, Development, evaluation and biodistribution of stealth liposomes of 5-fluorouracil for effective treatment of breast cancer, J. Liposome Res. 32 (2022) 146–158.
[37] H. Hinterwirth, S.K. Wiedmer, M. Moilanen, A. Lehner, G. Allmaier, T. Waitz, W. Lindner, M. Lämmerhofer, Comparative method evaluation for size and size-distribution analysis of gold nanoparticles, J. Separ. Sci. 36 (2013) 2952–2961.
[38] C.E. Schanté, G. Zuber, C. Herlin, T.F. Vandamme, Chemical modifications of hyaluronic acid for the synthesis of derivatives for a broad range of biomedical applications, Carbohydr. Polym. 85 (2011) 469–489.
[39] P. Butterworth, H. Baum, J. Porter, A modification of the Ellman procedure for the estimation of protein sulfhydryl groups, Arch. Biochem. Biophys. 118 (1967) 716–723.
[40] T. Ahmad, Reviewing the tannic acid mediated synthesis of metal nanoparticles, Journal of Nanotechnology 2014 (2014).
[41] H. Mühlpfordt, The preparation of colloidal gold particles using tannic acid as an additional reducing agent, Experientia 38 (1982) 1127–1128.
[42] L.L. Rouhana, M.D. Moussallem, J.B. Schlenoff, Adsorption of short-chain thiols and disulfides onto gold under defined mass transport conditions: coverage, kinetics, and mechanism, J. Am. Chem. Soc. 133 (2011) 16080–16091.
[43] H. Häkkinen, The gold–sulfur interface at the nanoscale, Nat. Chem. 4 (2012) 443–455.
[44] S. Gurunathan, J. Han, J.H. Park, J.-H. Kim, A green chemistry approach for synthesizing biocompatible gold nanoparticles, Nanoscale Res. Lett. 9 (2014) 1–11.
[45] C.-Y. Lee, W.-T. Wang, C.-C. Liu, L.-M. Fu, Passive mixers in microfluidic systems: a review, Chem. Eng. J. 288 (2016) 146–160.
[46] E. Kastner, V. Verma, D. Lowry, Y. Perrie, Microfluidic-controlled manufacture of liposomes for the solubilisation of a poorly water soluble drug, Int. J. Pharm. 485 (2015) 122–130.
[47] P. Srisuk, P. Thongnopnua, U. Raktanonchai, S. Kanokpanont, Physico-chemical characteristics of methotrexate-entrapped oleic acid-containing deformable liposomes for in vitro transepidermal delivery targeting psoriasis treatment, Int. J. Pharm. 427 (2012) 426–434.
[48] S. Joshi, M.T. Hussain, C.B. Roces, G. Anderluzzi, E. Kastner, S. Salmaso, D. J. Kirby, Y. Perrie, Microfluidics based manufacture of liposomes simultaneously entrapping hydrophilic and lipophilic drugs, Int. J. Pharm. 514 (2016) 160–168.

[49] A. Jahn, J.E. Reiner, W.N. Vreeland, D.L. DeVoe, L.E. Locascio, M. Gaitan, Preparation of nanoparticles by continuous-flow microfluidics, J. Nanoparticle Res. 10 (2008) 925–934.
[50] M. Ripoll, E. Martin, M. Enot, O. Robbe, C. Rapisarda, M.-C. Nicolai, A. Deliot, P. Tabeling, J.-R. Authelin, M. Nakach, Optimal self-assembly of lipid nanoparticles (LNP) in a ring micromixer, Sci. Rep. 12 (2022) 9483.
[51] S. Thamphiwatana, V. Fu, J. Zhu, D. Lu, W. Gao, L. Zhang, Nanoparticle-stabilized liposomes for pH-responsive gastric drug delivery, Langmuir 29 (2013) 12228–12233.
[52] D. Mori, T. Tsujikawa, Y. Sugiyama, S.i. Kotani, S. Fuse, G. Ohmura, A. Arai, T. Kawaguchi, S. Hirano, O. Mazda, Extracellular acidity in tumor tissue upregulates programmed cell death protein 1 expression on tumor cells via proton-sensing G protein-coupled receptors, Int. J. Cancer 149 (2021) 2116–2124.
[53] V. Fu, Nanoparticle Stabilized Liposomes for Acne Therapy, University of California, San Diego, 2013.
[54] H. Aghaei, A.R.S. Nazar, J. Varshosaz, Double flow focusing microfluidic-assisted based preparation of methotrexate–loaded liposomal nanoparticles: encapsulation efficacy, drug release and stability, Colloids Surf. A Physicochem. Eng. Asp. 614 (2021) 126166.
[55] B. Guldiken, M. Gibis, D. Boyacioglu, E. Capanoglu, J. Weiss, Physical and chemical stability of anthocyanin-rich black carrot extract-loaded liposomes during storage, Food Res. Int. 108 (2018) 491–497.
[56] J. Du Plessis, C. Ramachandran, N. Weiner, D. Müller, The influence of lipid composition and lamellarity of liposomes on the physical stability of liposomes upon storage, Int. J. Pharm. 127 (1996) 273–278.